university of groningen

University Medical Center Groningen

University of Groningen

The importance of crop growth modeling to interpret the Δ14CO2 signature of annual plants

Bozhinova, D.; Combe, M.; Palstra, S. W. L.; Meijer, H. A. J.; Krol, M. C.; Peters, W.

Published in:
Global Biogeochemical Cycles

DOI:
10.1002/gbc.20065

IMPORTANT NOTE: You are advised to consult the publisher's version (publisher's PDF) if you wish to cite from it. Please check the document version below.

Document Version
Publisher's PDF, also known as Version of record

Publication date:
2013

Link to publication in University of Groningen/UMCG research database

Citation for published version (APA):
Bozhinova, D., Combe, M., Palstra, S. W. L., Meijer, H. A. J., Krol, M. C., & Peters, W. (2013). The importance of crop growth modeling to interpret the Δ14CO2 signature of annual plants. *Global Biogeochemical Cycles*, *27*(3), 792-803. https://doi.org/10.1002/gbc.20065

Copyright
Other than for strictly personal use, it is not permitted to download or to forward/distribute the text or part of it without the consent of the author(s) and/or copyright holder(s), unless the work is under an open content license (like Creative Commons).

The publication may also be distributed here under the terms of Article 25fa of the Dutch Copyright Act, indicated by the "Taverne" license. More information can be found on the University of Groningen website: https://www.rug.nl/library/open-access/self-archiving-pure/taverne-amendment.

Take-down policy
If you believe that this document breaches copyright please contact us providing details, and we will remove access to the work immediately and investigate your claim.

Downloaded from the University of Groningen/UMCG research database (Pure): http://www.rug.nl/research/portal. For technical reasons the number of authors shown on this cover page is limited to 10 maximum.

Download date: 04-05-2023

GLOBAL BIOGEOCHEMICAL CYCLES, VOL. 27, 792–803, doi:10.1002/gbc.20065, 2013

The importance of crop growth modeling to interpret the $\Delta^{14}CO_2$ signature of annual plants

D. Bozhinova,[1] M. Combe,[1] S. W. L. Palstra,[2] H. A. J. Meijer,[2] M. C. Krol,[1,3] and W. Peters[1]

Received 19 March 2012; revised 11 April 2013; accepted 8 July 2013; published 30 August 2013.

[1] The $^{14}C/C$ abundance in CO_2 ($\Delta^{14}CO_2$) promises to provide useful constraints on regional fossil fuel emissions and atmospheric transport through the large gradients introduced by anthropogenic activity. The currently sparse atmospheric $\Delta^{14}CO_2$ monitoring network can potentially be augmented by using plant biomass as an integrated sample of the atmospheric $\Delta^{14}CO_2$. But the interpretation of such an integrated sample requires knowledge about the day-to-day CO_2 uptake of the sampled plants. We investigate here the required detail in daily plant growth variations needed to accurately interpret regional fossil fuel emissions from annual plant samples. We use a crop growth model driven by daily meteorology to reproduce daily fixation of $\Delta^{14}CO_2$ in maize and wheat plants in the Netherlands in 2008. When comparing the integrated $\Delta^{14}CO_2$ simulated with this detailed model to the values obtained when using simpler proxies for daily plant growth (such as radiation and temperature), we find differences that can exceed the reported measurement precision of $\Delta^{14}CO_2$ (~2‰). Furthermore, we show that even in the absence of any spatial differences in fossil fuel emissions, differences in regional weather can induce plant growth variations that result in spatial gradients of up to 3.5‰ in plant samples. These gradients are even larger when interpreting separate plant organs (leaves, stems, roots, or fruits), as they each develop during different time periods. Not accounting for these growth-induced differences in $\Delta^{14}CO_2$ in plant samples would introduce a substantial bias (1.5–2 ppm) when estimating the fraction of atmospheric CO_2 variations resulting from nearby fossil fuel emissions.

Citation: Bozhinova, D., M. Combe, S. W. L. Palstra, H. A. J. Meijer, M. C. Krol, and W. Peters (2013), The importance of crop growth modeling to interpret the $\Delta^{14}CO_2$ signature of annual plants, *Global Biogeochem. Cycles*, *27*, 792–803, doi:10.1002/gbc.20065.

1. Introduction

[2] Although observations of CO_2 have been very important for our current understanding of the carbon cycle [*Keeling*, 1978; *Tans et al.*, 1990; *Keeling et al.*, 1995; *LeQuere et al.*, 2007; *Stephens et al.*, 2007], it has proven difficult to extract process specific information from CO_2 alone. The observations are therefore usually complemented by observations of various trace gases connected with fossil fuel combustion, biosphere and ocean exchange (CO, $^{13}CO_2$, $^{14}CO_2$, SF_6, ^{222}Rn, O_2/N_2, and many others). Among the different alternatives, the radioactive isotope of carbon (^{14}C) is a tracer which is strongly influenced by anthropogenic CO_2 emissions. Its half-life time of 5730±40 years [*Godwin*, 1962] ensures that fossil fuel combustion releases only $^{12,13}CO_2$ into the atmosphere. This process effectively dilutes the atmospheric mixing ratios of $^{14}CO_2$ and is known as the Suess effect [*Suess*, 1955]. The magnitude of the dilution can thus be used to quantify regional fossil fuel CO_2 addition to the atmosphere in regions where this addition is of relatively large importance for $\Delta^{14}CO_2$.

[3] Usually, the method to calculate the recently added fossil fuel CO_2 (denoted from here on as CO_{2ff}) is based entirely [*Meijer et al.*, 1996; *Levin et al.*, 2003; *Turnbull et al.*, 2006; *Hsueh et al.*, 2007; *Palstra et al.*, 2008; *Turnbull et al.*, 2009; *Vay et al.*, 2009] or partly [*Gamnitzer et al.*, 2006; *Levin and Karstens*, 2007] on observations of CO_2 and $^{14}CO_2$. Atmospheric observations of $^{14}CO_2$ are typically reported as $\Delta^{14}CO_2$ (‰), the normalized difference between the sample and a standard, corrected for various processes [*Stuiver and Polach*, 1977; *Mook and van der Plicht*, 1999]. The total uncertainty in

[1]Department of Meteorology and Air Quality, Wageningen University, Wageningen, Netherlands.
[2]Centre for Isotope Research, University of Groningen, Groningen, Netherlands.
[3]Institute for Marine and Atmospheric Research Utrecht, Utrecht, Netherlands.

Corresponding author: D. Bozhinova, Department of Meteorology and Air Quality, Wageningen University, PO Box 47, NL-6700 AA, Wageningen, Netherlands. (denica.bozhinova@wur.nl)

©2013. American Geophysical Union. All Rights Reserved.
0886-6236/13/10.1002/gbc.20065

the calculation of CO_{2ff} mainly depends on the $\Delta^{14}CO_2$ measurement precision and can be less than 1 ppm per single observation for precision of ∼2‰ [*Turnbull et al.*, 2009]. Only few labs obtain such a precision, and in the more general case, where it is ∼3–5‰ the uncertainty in the recalculation will be between 1 and 2 ppm. Still, comparing this to the typical summer daytime CO_{2ff} at the site of Cabauw in the Netherlands (2–8 ppm) [*Tolk et al.*, 2009] or the CO_{2ff} in a polluted area like Heidelberg (10–12 ppm) [*Levin and Rodenbeck*, 2008] shows how $\Delta^{14}CO_2$ could provide useful information on regional fossil fuel emissions.

[4] Globally, $\Delta^{14}CO_2$ observations are collected only at a limited number of sites, with interest mostly toward the atmospheric background levels and thus usually far from anthropogenic emission sources [*Meijer et al.*, 1995; *Levin et al.*, 2010; *Graven et al.*, 2012]. To estimate the recently added fossil fuel CO_2 to the regional atmosphere, numerous flask samples or time-integrated samples should be taken from various sites [*Levin et al.*, 2003]. There are advantages and disadvantages to both sampling approaches, and besides the challenges in the measurement of ^{14}C itself, a major concern is the cost of long-term observations and sample analysis. A possible solution for the lack of observational sites is to use annual plant samples, as these have been shown to adequately represent in a qualitative manner the fossil fuel emissions on a continental [*Hsueh et al.*, 2007] and regional scale [*Riley et al.*, 2008]. Different types of annual plants are grown for agricultural and industrial use (for example, wine or rice production), often close to anthropogenic sources, thus offering an opportunity to obtain samples without significant financial investment. Additionally, because of the variable use of crops in industry, there is even the possibility to access information from previous years by sampling, for instance, wine records or rice grains [*Burchuladze et al.*, 1989; *Shibata et al.*, 2005; *Palstra et al.*, 2008].

[5] Integrated $\Delta^{14}CO_2$ samples obtained at most observational sites (among others, *Levin et al.* [1980] and *Meijer et al.* [1995]) differ substantially from plant samples. In the traditional method, atmospheric air is pumped for several weeks with constant flow rate through an alkaline solution (usually NaOH) that absorbs the CO_2 for later isotopic analysis. The absorbed CO_2 is thus proportional to the instantaneous CO_2 concentrations, and as the stable boundary layer traps the CO_2 emissions near surface overnight, this method usually weights nighttime periods more heavily [*Hsueh et al.*, 2007]. Even so, the interpretation of an integrated NaOH sample is relatively straightforward as its sampling period is fixed and its rate of sampling is constant. This differs considerably from plant samples, where the recorded signal is obtained only during daytime and both the growing/sampling period and assimilation rate vary substantially.

[6] Plant samples are usually obtained by picking leaves or storage organs (e.g., seeds and fruits) from annual, perennial plants or even from trees. In the study of *Hsueh et al.* [2007], the plant samples analyzed consisted mostly of corn leaves, but in some regions, also corn husks and annual forb were used. Their findings showed that the biomass of the annual plants represents a time-integrated measure of daytime atmospheric $\Delta^{14}CO_2$ during the period of growth, weighted by the rate of carbon fixation. In a further study, *Riley et al.* [2008] sampled winter annual grasses in California and compared the observed signatures with predicted ones. In this case, the modeled atmospheric $\Delta^{14}CO_2$ and modeled gross primary production (GPP) for C_3 grasses over the simulated area were used to estimate the $\Delta^{14}CO_2$ signature of the biomass, by creating a GPP-weighted sum of the daytime atmospheric signature. In the study of *Palstra et al.* [2008], grapes, and more specifically wine, were used as samplers. They discuss the difficulties arising from the unknown sampling period, and the variable carbon uptake flow and their modeling approach takes into account that grapes will form in only few months while the growing period of the grapevine is much longer. All these studies followed the idea that the atmospheric carbon isotope ratios are recorded as part of the daily photosynthesis and fixed in the plant structure when the assimilated carbon is allocated. Additionally, they agree that the period for which the atmospheric isotopic ratios are represented in the plant is related to the period and rate of growth of the plant. Thus, to quantitatively interpret a plant sample in the context of the atmospheric carbon isotope ratios, we must construct a function (averaging kernel) that weights the daily contribution of the atmospheric $\Delta^{14}CO_2$ signature to the signature of the entire integrated plant sample, or to the specific organ that was picked.

[7] It is clear that the averaging kernel has to be a function of the plant CO_2 assimilation rate, but the level of complexity in this kernel required for a reasonable representation of the signature is still unknown. The instantaneous rate of CO_2 assimilation depends on multiple factors, some of which are external to the plant (the abundance or absence of photosynthetically active radiation, the surface temperature and humidity, nitrogen application or disturbances) and some of which are internal (such as the plant species, phenological changes during the plant lifetime, and its drought sensitivity). In order to include plant observations to our suite of $\Delta^{14}CO_2$ sampling methods, we would like to reproduce the way plants sample atmospheric CO_2 and the resulting integrated $\Delta^{14}CO_2$ signature with sufficient accuracy. The latter is our objective in this paper.

[8] To isolate the effect of plant growth variations on the integrated $\Delta^{14}CO_2$ signature, we exclude in this study the other main source of variability that will be recorded: the fossil fuel emissions in the vicinity of growing plants. But our ultimate goal is to estimate exactly this fossil fuel component through the recorded $\Delta^{14}CO_2$ in plant samples. The plant growth averaging kernels described here thus form a barrier to this intended interpretation, and we show in this work how it can be overcome by using a suitable crop model to account for temporal and spatial plant growth variations over a growing season. To make the recorded atmospheric $\Delta^{14}CO_2$ in our simulated plants over a growing season as realistic as possible, but without any local fossil fuel influences, we have constructed one time series with realistic day-to-day $\Delta^{14}CO_2$ changes over a growing season to supply to all our calculations of plant sampled $\Delta^{14}CO_2$ over the domain we study, as described in section 2.1. The effects that we quantify here based on plant averaging kernel variations alone will be compared to expected fossil fuel (and other) signals from other published studies. We are working toward a full description of these variations for a follow-up study on the one presented here.

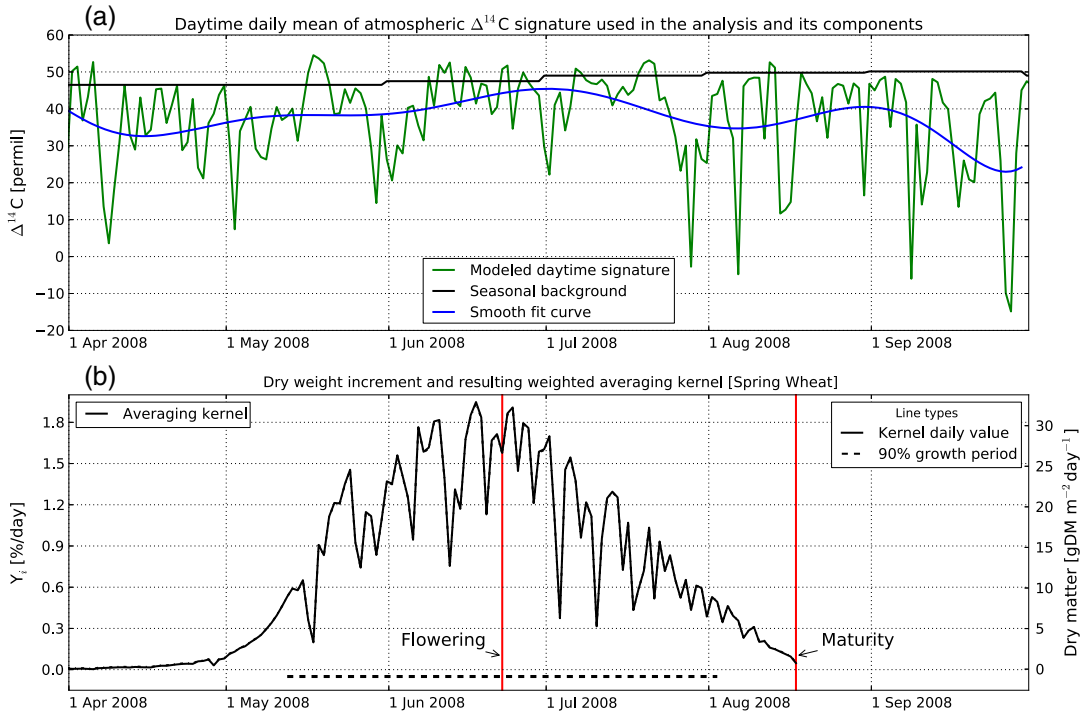

Figure 1. (a) Simulated daily averaged daytime-only atmospheric $\Delta^{14}CO_2$ signature over the Netherlands (in green). The series are estimated using observed 2008 hemispheric background $\Delta^{14}CO_2$ values from Jungfraujoch [*Levin et al.*, 2010] (in black) and local fossil fuel addition modeled using CarbonTracker results for the location of Lutjewad (Netherlands). The smooth curve was created using NOAA Earth System Research Laboratory's ccgcrv routine [*Thoning and Tans*, 1989] (in blue). (b) Total plant dry weight increment and resulting averaging kernel for spring wheat, modeled with SUCROS 2 and weather data from Wageningen (Netherlands). The averaging kernel is complemented by estimation of the 90% growing period (dashed horizontal line at bottom of the figure).

[9] Specific questions that we address in this work are: (1) Which external data do we need to accurately construct an averaging kernel for plant samples? (2) Are there sampling or interpretation-related strategies that minimize the sensitivity of the resulting $\Delta^{14}CO_2$ signature to the averaging kernel? (3) Can a simple proxy for plant growth reasonably replace the more complex modeling of the crop growth pattern over time? And finally, (4) can the use of detailed plant growth models overcome the possibly limited interpretability of plant samples for fossil fuel monitoring?

2. Methodology

2.1. The Modeled Atmospheric $\Delta^{14}CO_2$ Signature

[10] To investigate the sample signatures resulting from the use of different averaging kernels, we construct one time series with realistic variations of the atmospheric $\Delta^{14}CO_2$ evolution on an hourly scale. This time series we prescribe to all the locations and kernels we use in this study to simulate integrated samples. We constructed this time series based on the regional budget of the atmospheric $\Delta^{14}CO_2$, and the estimation of recently added fossil fuel CO_2 as also used in *Levin et al.* [2003], *Turnbull et al.* [2006], *Hsueh et al.* [2007], *Riley et al.* [2008], *Palstra et al.* [2008], and *Graven and Gruber* [2011] and thoroughly described in *Turnbull et al.* [2009]. The simplified form of the calculation is shown in equation (1).

$$\Delta_{sample} = \frac{\Delta_{bg}(CO_{2sample} - CO_{2ff}) + \Delta_{ff}CO_{2ff}}{CO_{2sample}} \quad (1)$$

[11] Here the observed atmospheric $\Delta^{14}CO_2$ signature (Δ_{sample}) is described through a relation between the total observed CO_2 concentrations ($CO_{2sample}$), the background CO_2 concentrations (CO_{2bg}, consisting of biospheric, oceanic, fire derived, and nonrecent fossil CO_2 emissions) and the recent fossil fuel addition (CO_{2ff}), with their respective $\Delta^{14}CO_2$ signatures (Δ_{bg},Δ_{ff}). Thus calculated, our atmospheric $\Delta^{14}CO_2$ series excludes the influence of the nuclear power plant production, ocean disequilibrium and biosphere disequilibrium fluxes, and of ^{14}C-enriched high tropospheric and stratospheric air (all to the extent that they are not represented in the background terms). While these processes should be accounted for when actually interpreting observed $\Delta^{14}CO_2$ samples, in our current work, they are of less importance as the fossil fuel addition has much greater influence on the day-to-day variability.

[12] Time series of CO_{2ff}, CO_{2bg}, and $CO_{2sample}$ (where $CO_{2sample}$= CO_{2bg}+CO_{2ff}) with 1.5 h temporal resolution were simulated for the Lutjewad sampling station (Centre for Isotope Research, Groningen University, Netherlands;

Table 1. Statistical Comparison Between Observational Data From 35 Stations in the Netherlands (Royal Netherlands Meteorological Institute (KNMI), http://www.knmi.nl) and WRF-Simulated Weather for Each Station Location[a]

Daily Weather Variable (Units)	$\overline{O-P}$	$\overline{O-P}/\overline{O}$ x100%	σ_{O-P}	RMSE	r
Solar radiation (W m^{-2})	–45.27	–24.3	61.9	76.86	0.65
Minimum temperature (°C)	0.04	0.4	2.7	2.84	0.81
Maximum temperature (°C)	–2.11	–10.9	2.1	2.94	0.90
Water vapor pressure (kPa)	0.1	7.5	0.2	0.19	0.90
Mean wind speed (m s^{-1})	–0.94	–22.0	1.22	1.72	0.75
Precipitation (mm d^{-1})	0.3	14.4	5.0	5.02	0.37

[a]Shown are the results for the root mean square error (RMSE), correlation coefficient (r), and the absolute ($\overline{O-P}$) and relative ($\overline{O-P}/\overline{O}$ ×100%) differences between observed and predicted means and the standard deviation of the difference between observed and predicted (σ_{O-P}). Negative differences in the mean values occur when the model is predicting higher values than observed. The relative difference is expressed in [%], the correlation coefficient is unitless and all other measures refer to the units described in the first column.

latitude 53°24′N, longitude 6°21′E, altitude 1 m above sea level (asl); henceforth Lutjewad), based on CarbonTracker Europe modeling results [*Peters et al.*, 2010]. The fossil fuel emissions use the annual global and country totals from the Carbon Dioxide Information and Analysis Center [*Marland et al.*, 2008], spatial distribution on national level according to the patterns of Emission Database for Global Atmospheric Research [*Olivier and Berdowski*, 2001] v4.0 and the seasonality per grid box is dependent on the inventory of the Institute of Economics and the Rational Use of Energy [*Pregger et al.*, 2007], University of Stuttgart - more details are available on http://www.carbontracker.eu. The choice of location is somewhat arbitrary, since we will apply the same time series uniformly for our entire spatial domain, but we decided on this location as it provides observational data from integrated monthly $\Delta^{14}CO_2$ samples. We estimate monthly averaged Δ_{bg} from observed time series for the Jungfraujoch site [*Levin et al.*, 2010]. Fossil fuels are totally devoid of $^{14}CO_2$, and as such, their signature is $\Delta_{ff} = -1000‰$. Together with equation (1), these simulated and observed values allowed us to construct a realistic diurnal $\Delta^{14}CO_2$ time series.

[13] The atmospheric $\Delta^{14}CO_2$ signature seen by the plants is always the signature of the sunlit part of the day, when the boundary layer is developed and usually well mixed. For the actual application of the atmospheric time series, we created daytime averages from the available daily data for the hours between 0600 and 2000 local time (LT) every day starting from 1 April and ending with 30 September 2008. The constructed time series for daytime daily $\Delta^{14}CO_2$ is shown in Figure 1a along with the observed Δ_{bg} from Jungfraujoch (as applied in our calculations) and a smooth curve fit [*Thoning and Tans*, 1989] to our full time series. The figure shows that day-to-day variations in $\Delta^{14}CO_2$ are large compared to month-to-month variations visible in the smoothed curve.

2.2. SUCROS Model Description

[14] We use the Simple Universal Crop Growth Simulator 2 (SUCROS 2) to model plant growth and associated CO_2 uptake [*Goudriaan and van Laar*, 1994; *van Laar et al.*, 1997]. SUCROS 2 is a mechanistic model that includes the main processes of carbon assimilation, such as photosynthesis and autotrophic (growth and maintenance) respiration. It simulates the crop dry matter accumulation in water-limited conditions but does not account for nutrient limitation, pests, diseases, and weed effects on growth. SUCROS 2 has the advantage of simulating plant phenology and as a result has a development-dependent carbohydrate partitioning and leaf area index. The model has been applied to several crops (wheat [*van Laar et al.*, 1997], maize [*Xevi et al.*, 1996; *Arora and Gajri*, 2000], sugar beet [*Guérif and Duke*, 1998], sugar cane [*Singels et al.*, 2010], and cotton [*Zhang et al.*, 2008]) and has evolved as the platform on which more complex and specialized models are built [*van Ittersum et al.*, 2003].

[15] SUCROS 2 simulates the growth of a field of specific plant species, and in this research, we have modeled the growth of two common crops—maize (*Zea mays*) and spring wheat (*Triticum aestivum*). We chose these two species for their large use in agriculture and because they are widely grown not only in the Netherlands but most parts of the world. As they are of great interest for the food industry, there is an abundance of research and field data available to validate models for these crops, including SUCROS 2. Additionally, these two crops grow in similar conditions and consecutive periods in the year, opening the possibility for sampling scenarios that use multispecies samples to provide observations for longer period of time.

[16] Besides the species specific physiological and phenological characteristics, the model requires limited information about the initial conditions of the crop growth and general daily weather information for the location in question. For the species that we chose to investigate, water stress is rarely of importance before the flowering stage. The input weather data is described in more detail in section 2.3.

[17] In SUCROS 2, the different plant organs are represented as separate pools of dry mass for leaves, roots, stems, and storage organs. In this study, we investigate the dry weight increment for each of these organs, and for the entire plant, to use as kernels to express the CO_2 assimilation by the plant. The biggest change in growth dynamics of the chosen plant species occurs at flowering. This stage marks the end of the vegetative growth of the plant, and the beginning of the reproductive phase, when the development and growth of storage organs takes priority over all other plant part compartments. In cereals, the plant will translocate biomass from stems and leaves to the storage organs, usually starting after the flowering stage. This process is captured by SUCROS 2 but is difficult to account for when modeling the recording of the $\Delta^{14}CO_2$ signature over time. We will further comment on the development driven differences that occur during the lifetime of the plant, as they are important for the $\Delta^{14}C$ signature of the plant and its organs.

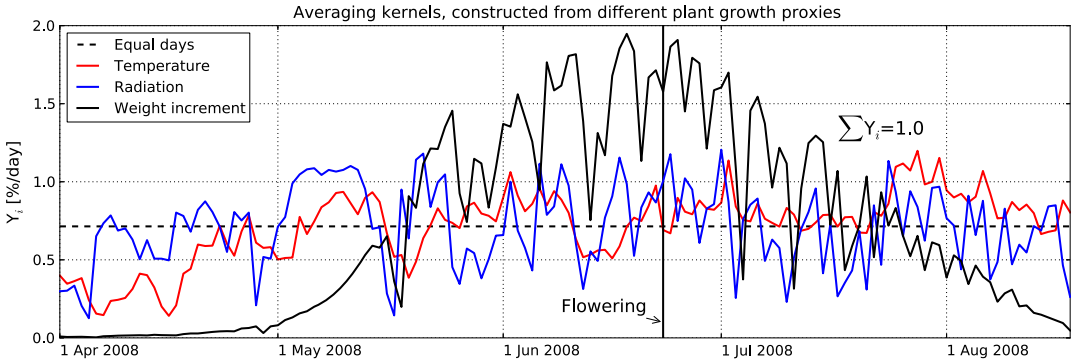

Figure 2. Examples of possible averaging kernels constructed for a given growing season for the location of Haarweg (Netherlands). Each solid line represents a different proxy for plant growth, as opposed to a kernel of equally weighted days (dashed). Both temperature and radiation are taken from station observations and are also used as input to the SUCROS 2 crop growth model that returns the daily dry weight increment (here shown for spring wheat) to which the other kernels are compared in the text.

2.3. Weather Data

[18] Observed and simulated weather for the year 2008 over the Netherlands was used as input for the SUCROS 2 crop growth model. Observational data was taken from the Haarweg meteorological station (Meteorology and Air Quality group, Wageningen University, Netherlands; latitude 51°58′N, longitude 5°38′W, altitude 7 m asl; www.maq.wur.nl) and used to investigate the plant growth characteristics at a single location (sections 3.1 and 3.2). To get spatially explicit weather data for the growing season between 1 April and 1 October 2008, we used the Weather Research and Forecast (WRF) model. A detailed description of WRF is available in *Skamarock et al.* [2008]. The WRF-generated weather data is used in section 3.3. To prevent confusion, we explicitly state that the WRF model was not used for any atmospheric transport of tracers, or CO_2, or its isotopes, but only to generate meteorological variables to drive plant growth.

[19] The WRF model was initialized using boundary conditions from 6-hourly global reanalysis fields from the National Centers for Environmental Prediction - National Center for Atmospheric Research [*Kalnay et al.*, 1996], for three two-way nested domains with the number of total grid points of 60×60/52×52/88×88 and corresponding horizontal resolution of 36/12/4 km. The vertical resolution was 28 levels, with 15 levels in the lower 2 km and 6 levels in the first 200 m of the atmosphere. The model setup included the Monin-Obukhov surface layer physics scheme, the Unified Noah land-surface model [*Ek et al.*, 2003] and the Yonsei University planetary boundary layer scheme [*Hong et al.*, 2006]. The resulting output that was used in this study has an hourly temporal resolution over the nested domain with spatial resolution of 4×4 km (88×88 grid points).

[20] The WRF results were compared to observational data from 35 meteorological stations in the Netherlands (Royal Netherlands Meteorological Institute (KNMI), http://www.knmi.nl) to estimate the quality of the simulated weather conditions during the growing season. The daily weather input for the SUCROS 2 model, constructed from station observed data and the WRF simulation, was evaluated on a statistical basis through comparison between observed and predicted mean values, standard deviations, root mean square error (RMSE), and Pearson's correlation coefficient (r)—methods described in *Willmott* [1982]. A selection of these results is shown in Table 1. Overall, our comparison shows that the WRF-simulated weather is close to the one observed in the local meteorological stations. The two variables in which we see largest differences during the 6 months of simulated weather are the daily radiation sum and daily precipitation sum. In both cases, the reason for the difference is the general difficulty, found also in other mesoscale models, to model the cloud formation and rain events at a particular location. On average, for the 6 months of weather simulation, this results in overprediction in the amount of daily radiation and underprediction in the daily precipitation. We assess that the difference in the radiation would add a slight bias in our total simulated plant growth, which, however, does not affect the day-to-day variations. The underprediction of both precipitation and mean wind speed could result in limiting plant growth conditions. Nevertheless, for the plant species we investigate, water stress occurs mostly after the flowering date, which is a growth period we do not analyze in depth, as discussed in section 4.

Table 2. Final Signatures at Flowering and at the End of the Growing Period (Maturity)—$\Delta^{14}C_{res}$ (‰)[a]

	Spring Wheat		Maize	
$\Delta^{14}C_{res}$(‰)	Flowering	Maturity	Flowering	Maturity
Leaves	39.0	39.0	39.6	39.6
Roots	38.6	38.8	39.6	39.5
Stems	41.0	41.3	42.6	41.7
Storage organs	-	40.6	-	38.1
Total plant	40.5	40.8	41.4	39.5
Flat kernel	37.8	38.3	38.4	38.9
Radiation	37.6	38.0	38.4	38.4
Temperature	37.6	37.8	38.3	38.5

[a]We compare here averaging kernels for different plant parts and plant growth proxies, for spring wheat and maize. The kernels for the proxies are constructed using the same period in which the plant growth occurs.

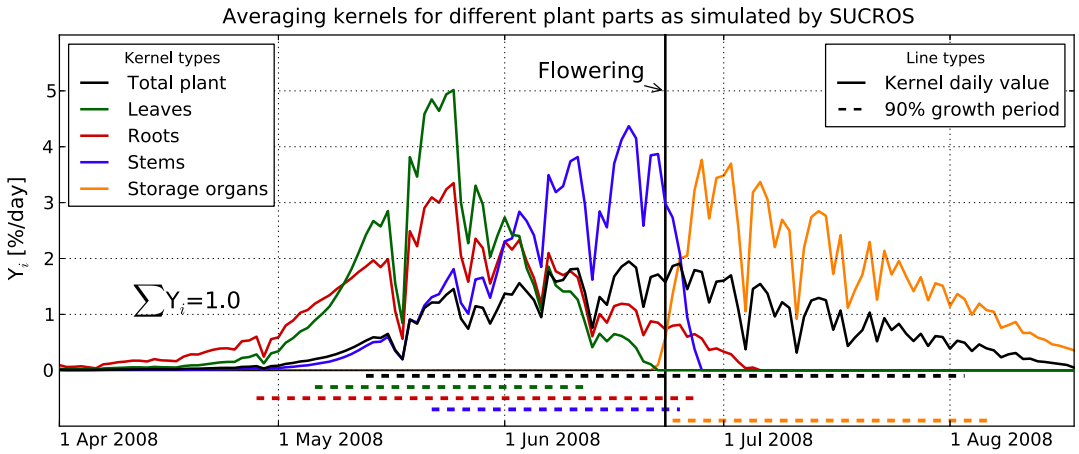

Figure 3. Averaging kernels constructed for different plant organs in comparison to the total plant kernel, all modeled with SUCROS 2 for spring wheat for the location of Haarweg. Plant part kernels are based on the daily dry weight increment and complemented with estimation of the according 90% growth periods (dashed lines).

2.4. The Averaging Kernels

[21] To translate the atmospheric $\Delta^{14}C$ signal into the integrated $^{14}CO_2$ signal in plants, we construct an averaging kernel (Y) of a time series (X) by normalizing the value of each element toward the sum of all the elements of a chosen period. Thus, the daily value of the kernel (Y_i) is expressed as follows:

$$Y_i = \frac{X_i}{\sum_t X_i}. \quad (2)$$

After the application of the averaging kernel to the atmospheric $\Delta^{14}CO_2$ series ($\Delta^{14}C_{sample}$ or Δ_{sample}), the resulting integrated signature ($\Delta^{14}C_{res}$ or Δ_{res}) will be

$$\Delta^{14}C_{res} = \sum_t \Delta^{14}C_{sample i} Y_i. \quad (3)$$

[22] The kernel constructed from SUCROS 2-simulated daily dry weight increment is treated in this study as the "true kernel" as it represents the most complete simulation of all factors affecting plant growth simultaneously. In addition, we also constructed a flat kernel (representing an equal-weighted mean of the atmospheric $\Delta^{14}CO_2$ signature), and kernels from daily incoming solar radiation and 2 m temperature as these are known to strongly influence plant growth.

[23] We constructed separate averaging kernels for the plant organs (leaves, stems, roots, and storage organs) from the daily dry weight increment of the respective compartments. We calculated the signatures resulting from these kernels for the period that ends when the plant reaches the flowering stage, and at the end of the growing period, when the plant reaches maturity. We define the peak period of an averaging kernel as the period, in which 90% of the growth of the plant is occurring, by removing the periods of lower relative weight. Hereafter, we refer to this period as the peak period, or the 90% period. The true kernel for the total plant simulation of spring wheat and the according 90% period can be seen in Figure 1b.

3. Results

[24] In the following sections, we will address three main research questions of this study.

3.1. Can a Plant Growth Proxy Replace a Plant Growth Model?

[25] Daily plant growth is closely connected to the weather variables chosen as proxies (daily radiation sum and mean daily temperature), but the resulting averaging kernels have fundamentally different distributions (Figure 2). The weather-based proxies lack the bell-shape of the "true" (SUCROS 2-produced) kernel based on dry matter increment. This difference already suggests that plant samples represent the atmospheric signature for a period smaller than the entire growing season of the plant. During the peak growing season, the correlation with incoming solar radiation is highest (Pearson's coefficient r = 0.60 with 1 day lag) as we would expect from basic plant physiology. This correlation increases to r = 0.90 if we only analyze the period between mid-June to mid-July. Temperature does not correlate well with dry matter increment (r = –0.09 for peak period, r = 0.12 for June-July). This means that the variance of daily dry matter increment is generally not captured well by the weather proxies over the growing season.

Table 3. Mean and Standard Deviation (σ) of the Difference in $\Delta^{14}C$ Signature in Different Plant Compartments at Flowering (Upper Half) and Maturity (Lower Half) Using 30 Permutations of the 2008 Atmospheric $\Delta^{14}C$ Signature at Lutjewad[a]

Absolute Difference in $\Delta^{14}C_{res}$ [‰]	Spring Wheat		Maize	
	Mean	σ	Mean	σ
Leaves – stems	3.0	1.5	2.1	1.2
Leaves – roots	0.8	0.4	0.2	0.2
Roots – stems	2.5	1.0	2.0	1.2
Leaves – storage organs	4.8	2.5	5.7	2.3
Roots – storage organs	3.9	2.1	5.7	2.4
Stems – storage organs	3.4	2.7	4.8	2.4

[a]The signature of storage organs is calculated by analogy to other plant organs, thus ignoring the effects of translocated stem dry mass.

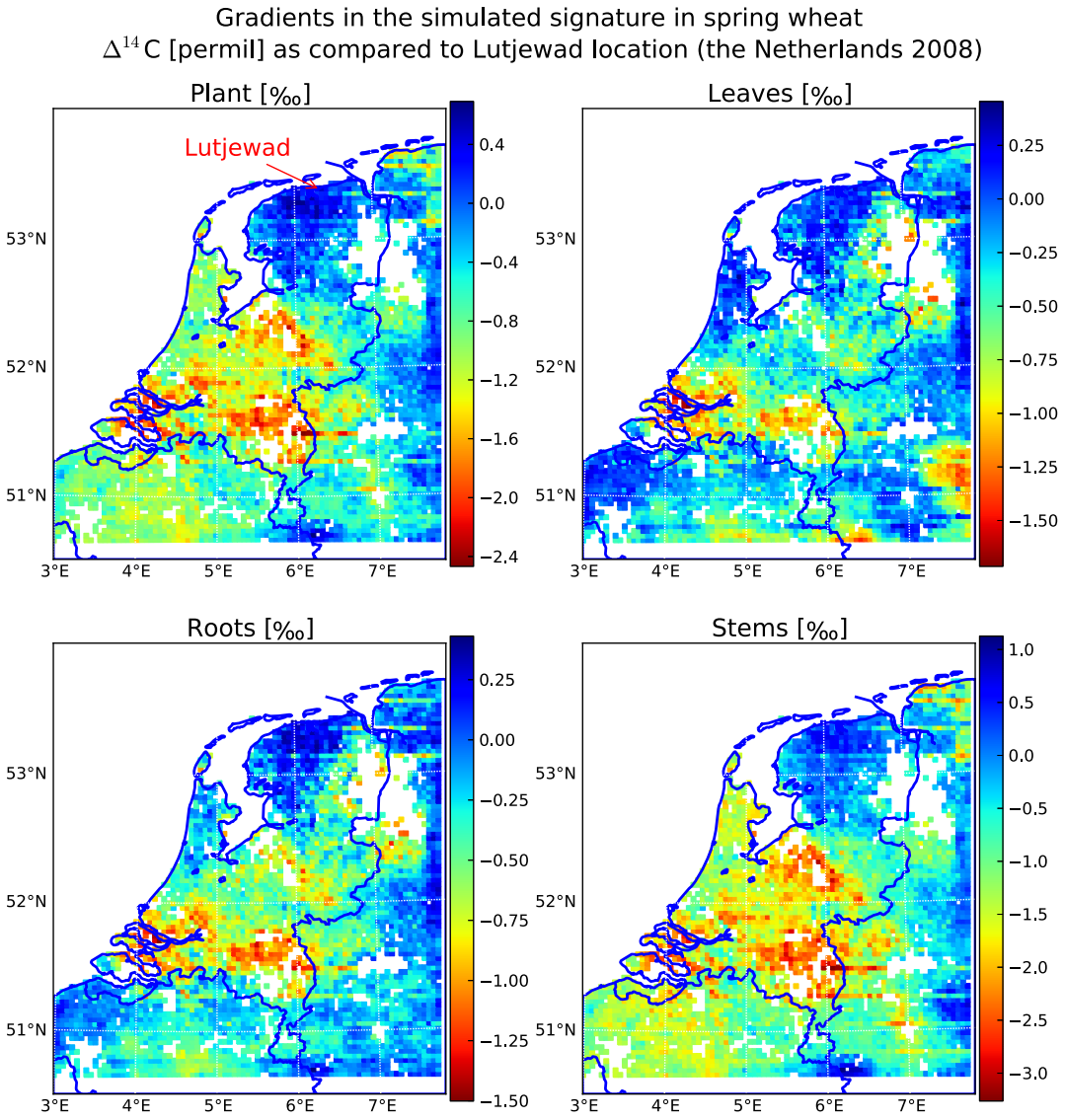

Figure 4. Spatial gradients of the simulated $\Delta^{14}C$ signature in spring wheat at flowering, constructed by subtracting the signature at each location from the one simulated at Lutjewad (red arrow). The gradients result only from different growth patterns induced by regional weather differences, as the temporal evolution of the atmospheric $\Delta^{14}C$ signature is unified over the entire domain. These gradients will superimpose on gradients from local fossil fuel emissions, resulting in biases when the fossil fuel addition is calculated back from observed plant samples if the plant growth differences are ignored. Each panel shows a different plant part sampled.

[26] When these kernels are combined with our simulated $^{14}CO_2$ time series, the resulting difference in the integrated $\Delta^{14}CO_2$ signature can be as small as 0.6‰ and as large as 3.1‰. Table 2 shows the full results. For example, signatures at the flowering stage range from 38.6‰ to 41.0‰ for spring wheat samples, and from 39.6‰ to 42.6‰ for maize, depending on the kernel applied. This range becomes larger when extending the sampling period to maturity.

3.2. Can We Interpret Samples From Different Plant Organs?

[27] An additional advantage of using a plant growth model like SUCROS 2 to construct the averaging kernel instead of a simpler growth proxy is the opportunity to account for plant phenology. An example is the partitioning of carbohydrates between different plant parts. Even in a model with very simple phenology such as SUCROS different plant organs grow in different periods during the growing season (Figure 3). The organs thus integrate the signal of the atmospheric $\Delta^{14}CO_2$ from different temporal windows, and this may result in internal signature gradients in the plant.

[28] We simulate internal gradients as large as 3.5‰ if we include storage organs in our analysis. Typical values of 2–3‰ are found if we limit our analysis to the organs growing before the flowering stage (leaves, roots, and stems). The largest absolute gradients before flowering are

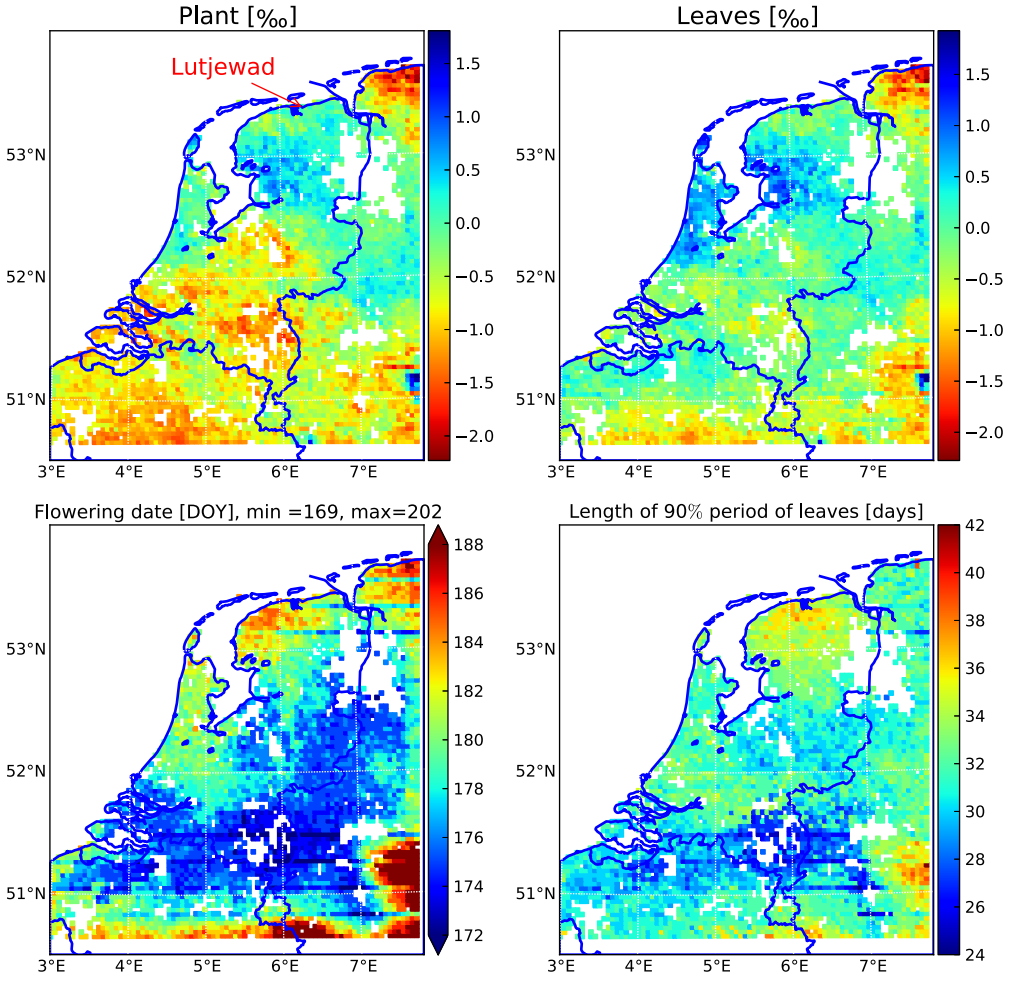

Figure 5. Top two panels are respective to Figure 4, but modeled for Maize. The bottom panels additionally show differences in the flowering date occurrence and length of the period with 90% growth of leaves. Growing season differences are caused by differences in the regional weather patterns, which affect the crop development and growing pattern.

found between the stems and the roots/leaves (see Table 2). This is true for both species, and results simply from the later development (the 90% period) of the stems by about 1 month. Leaves and roots both have their peak development at the same time and gradients therefore typically remain small (<0.5‰). We note, however, that the sampling of roots in the field is a very impractical approach. Leaves thereby remain the only practical organ to sample and interpret, though we note that for this example of growing season in our study, their signature is up to 1.8‰ different from the one accumulated in the whole plant, and also close to 1‰ different from the equal atmospheric average.

[29] Finally, we calculated the sensitivity of these internal gradients toward the simulated atmospheric $\Delta^{14}C$ series by shifting the original time series 30 times by increasing intervals from 2 to 60 days. This resulted in the calculated uncertainty (1-σ) in Table 3. Although the absolute plant signature (not shown) depends on the temporal evolution of the atmospheric $\Delta^{14}C$ series used, the internal gradients were persistent and on average of measurable size for most compartments.

3.3. How Does the Averaging Kernel Affect Gradients on the Regional Scale?

[30] Local weather can be consistently different on a regional scale, creating variable crop growing patterns and timing. We investigated the effect of these differences on the $\Delta^{14}CO_2$ signature for plants across the Netherlands. For this purpose, we combined WRF-generated weather for each point on the model 4 km grid with the plant growth of the SUCROS 2 model, and applied the resulting dry matter increment averaging kernels to the simulated atmospheric $\Delta^{14}C$ for Lutjewad (section 2.1). This simulation of the plant $\Delta^{14}C$ signature thus *excludes* any gradients of fossil fuel

emissions within the domain. Instead, it shows the spatial gradients in the plant signature that result solely from the different plant growth rates, which in turn are driven by the spatial differences in the weather conditions. We show the results (Figures 4 and 5) as a difference between the signature at flowering at each grid point and the location of Lutjewad, rather than as an absolute value.

[31] Differences in plant growth rates resulted in spatial $\Delta^{14}C$ gradients of over 2.5‰ for a total plant sample, and from 1.7‰ to over 4‰ for separate plant organs for spring wheat (Figure 4). For maize, we simulated more than 3.5‰ spatial gradients in the total plant samples, and up to 4.0‰ for the separate plant organs (Figure 5). The difference in gradients when considering different organs depends on species-specific crop development rates and the atmospheric $\Delta^{14}CO_2$ evolution. As an example, predicted flowering dates within the Netherlands vary by more than $\pm$6 days for spring wheat and more than $\pm$8 days for maize, even with explicitly forced emergence (start of growing period) at the same date over the entire domain. Even with a unified $\Delta^{14}CO_2$ time series to record, the plants thus accumulate gradients that can exceed the usual measurement precision, and this gradient will likely be even larger if we also allow realistic ($\pm$30 days) differences in the sowing date of crops across the country.

[32] We additionally evaluated the differences between the plant and atmospheric mean $\Delta^{14}C$ signature using Δ_{bg} only, the full daytime series and its smooth curve fit and residual components (all shown earlier in Figure 1). This allows us to quantify the contribution of each component of the $\Delta^{14}C$ time series to the total plant-atmosphere difference. Our calculations show that whether one applies a plant or a flat kernel to the seasonal background has very little impact on the signature (<0.4‰). Much larger differences arise from applying the kernels to the smooth curve (monthly variations) and to the residuals (daily variations). We calculate that the monthly time scales dominate and typically lead to a signature that is $\sim$2–3‰ higher in the plant samples than in the atmosphere. This strong effect is partly countered by the residual daily variations (mostly negative) which are more strongly expressed in plants than in the atmosphere. Together, this leads to a difference of about 1.7$\pm$0.5‰ when applying each kernel to the total time series. This suggests that both components of variation must be accounted for when interpreting plant sampled $\Delta^{14}CO_2$.

4. Discussion

[33] We investigated the requirements on simulating averaging kernels to properly interpret a plant sampled $\Delta^{14}CO_2$ signature. We compared the very complex kernel (modeled plant growth using SUCROS 2) with very simple ones (observed weather variables) and a temporally flat kernel. Results for these kernels (section 3.1) are generally comparable, but 1–2‰ different from the simulation of the signature of leaves with the complex growth model. Leaves are the plant parts previously used for analysis [*Hsueh et al.*, 2007]. Quantitatively, our study suggests that using a plant growth proxy that does not account for the day-to-day variations in plant growth comes at a price which varies from a possibly acceptable bias in $\Delta^{14}C$ ($\sim$0.5‰) to an absolutely unacceptable one (>3.0‰). We note that as the measurement precision of $\Delta^{14}CO_2$ increases, even a smaller bias might become unacceptable.

[34] An alternative kernel that is between the simple and complex extremes mentioned above, is one constructed from the leaf area index (LAI). LAI is a result of plant growth and additionally has the attractive advantage of being available over large areas from remote sensing. A step further toward complexity stands gross primary production (GPP) modeled from LAI observations. For some plant species, this approach has proven to give reasonable results, for instance in the case of annual grasses [*Riley et al.*, 2008]. We tried to investigate these proxies using monthly LAI data at $1^\circ \times 1^\circ$ spatial resolution (constructed from Global Inventory Modeling and Monitoring Study normalized difference vegetation index with 8 km/15 days resolution, source: K. Schaefer), Moderate Resolution Imaging Spectroradiometer observed LAI with 1 km/8 days resolution (MOD15A2) and high-resolution (250 m/1 day) spatial maps of GPP for the Netherlands [*Kooistra et al.*, 2009]. However, satellite observations depend on the lack of cloud cover, which results in periods where data is not available or is averaged over time, and we found it nearly impossible to construct data-based proxies for a full growing season for more than a few locations. Additionally, the data obtained is spatially averaged over the area covered by a pixel and would average signals from different plants species and from plants at different development stages. This is a significant drawback because neighboring crop fields can have up to a month difference in the sowing date even if they are from the same species. In the end, we did not include these mostly failed attempts with remotely sensed GPP and LAI in the paper. We did, however, construct one simulated LAI time series from the plant growth model to use but found it to perform poorly compared to the full growth model, with differences in the simulated total plant signature varying from 0.3‰ for wheat to 0.8–1.6‰ for maize.

[35] One of the questions arising for the general application of the growth averaging kernel is if it can be replaced by fitted curve that resembles the parabolic shape of the kernel and avoids the complication of using a crop growth model. As visible from Figure 3, the kernels for different plant parts differ substantially in their amplitude, skewness, the timing of the maximum, even in the case shown where the shape of the kernel is not seriously modified by limited growth periods. To construct a curve for a kernel, we would need to know at least the period of the intensive growth, the time when the maximum occurs and the peak amplitude. These parameters would differ per plant species and growing conditions in different time periods or locations. We are unaware of a method that can obtain this information while avoiding the use of a crop growth model itself.

[36] We evaluated the uncertainty in our plant $\Delta^{14}C$ signature results ($\Delta^{14}C_{res}$) introduced by the uncertainty in the model forcing (weather and initial conditions) data. Random errors of up to 25% in the weather variables did not produce significant change in our resulting signature. The biggest sensitivity found in our results ($\sim$1.0‰) was due to changes in the sequences of weather that follow each other over the entire growing season (synoptic variability). Consequently, we advise to interpret plant samples using appropriate growing season weather and avoid using an average climate year.

[37] Interestingly, differences in weather from location-to-location as presented in section 3.3 have a much larger effect on $\Delta^{14}CO_2$ than the changes in local weather from day-to-day, mentioned above. The resulting "growth-gradients" in the $\Delta^{14}CO_2$ signature of plant samples will superimpose on the atmospheric gradients by regional fossil fuel emissions that we are ultimately planning to interpret from the plants. Using again equation (1), the gradients in $\Delta^{14}CO_2$ will be equivalent to CO_{2ff} gradients of close to 1.5 ppm. This bias is of considerable size when compared to, for instance, the average fossil fuel CO_2 fraction during daytime at the site of Cabauw (2–8 ppm) in the Netherlands [*Tolk et al.*, 2009] or Heidelberg (10–12 ppm) in Germany [*Levin and Rodenbeck*, 2008] and is likely to be even larger when differences in sowing date (now excluded) are incorporated. Thus, the influence of local plant development rates as modified by local weather conditions during the growing season cannot be ignored when interpreting integrated samples.

[38] The next most used tracer for fossil fuel emissions after $^{14}CO_2$ is carbon monoxide (CO). *Gamnitzer et al.* [2006] estimates the uncertainty when using this tracer to be within ±20–35% of the recalculated fossil fuel CO_2. For the summertime period when plant samples are most easily available though, the uncertainties in the CO method are even higher, as the photochemical production, biomass burning, and OH consumption of CO, are most significant in summer [*Turnbull et al.*, 2006]. This suggests that plant $\Delta^{14}CO_2$ samples can be a useful addition to other tracer samples obtained to constrain regional fossil fuel CO_2 emission estimates.

[39] Various studies used plant-sampled $\Delta^{14}C$ from different plant parts and different species of grasses, cereal crops, forbs, or grapevines [*Burchuladze et al.*, 1989; *Shibata et al.*, 2005; *Hsueh et al.*, 2007; *Palstra et al.*, 2008; *Riley et al.*, 2008]. There are difficulties comparing the data between different studies, when the period and rate of carbon uptake is unknown or not taken into account. The use of a crop growth model allows for comparison when interpreting $\Delta^{14}C$ results from samples from different locations, sampling approaches, and materials or different time periods. In studies that use various types of samples, crop modeling should be a requirement to separate the effects of the atmospheric $\Delta^{14}CO_2$ signal and the different crop development and growing period.

[40] In our work, we focused on results obtained from plant samples at flowering and not as much for samples of storage organs at maturity. In cereal crops, such as spring wheat and maize, the storage organs (seeds) are different from the other organs in three important ways: (1) they grow exclusively after flowering, when (in cereal species) the other organs stop growing, (2) they grow partly from biomass that is reallocated from the other organs, rather than purely from newly assimilated carbon, and (3) the period after flowering shows much larger influence of weather variations (water limitations) on plant growth. Together, this makes $\Delta^{14}CO_2$ in storage organs difficult to relate to atmospheric $\Delta^{14}CO_2$. For instance, reallocation of biomass from stems to storage organs in our study accounted on average for 15% of the final biomass in that organ pool, introducing an $\Delta^{14}CO_2$ signature from an earlier growing stage. Our calculation of the resulting signature (equation (3)) does not account for this influence, and the uncertainty of our results for $\Delta^{14}C_{res}$ of storage organs is much higher than for other plant organs. In other plant species, the biomass dynamics could be quite different. For example, in grapevines, the reallocation of biomass happens before flowering, and the fruits grow almost exclusively from freshly assimilated CO_2. Such differences should be carefully considered when choosing the plant species and material that will be sampled.

[41] As a result of our work, we advise different plant parts to be obtained and analyzed separately, rather than a mixed sample. This is advantageous when their growth pattern is modeled, and it allows to correctly interpret samples from different plant parts, rather than assuming that they have the same signature as the total plant, as has been done up to now. Local farmers choose their sowing dates depending on local weather and other practical reasons. This results in up to a month differences in the development in neighboring fields of same species with different owners. This further implies that in order to be able to interpret plant observations, we should model the plant growth at the sampling location with the specific initial conditions.

[42] The next step in our research is to combine our crop growth model with simulations of the regional fossil fuel emissions and atmospheric transport. Once the regional weather is simulated, we can model the crop growth for locations where samples were previously obtained, and compare the predicted signature and gradients with observed ones. Our method might be advantageous for deciding which samples we want to analyze, as we will be able to predict the magnitude of expected gradients between plant samples.

5. Conclusions

[43] In our study, we constructed averaging kernels that allow us to calculate the $\Delta^{14}CO_2$ signature of a plant by making a weighted average of the daily contribution from the atmospheric $^{14}CO_2$ mixing ratios. This kernel needs to be known with sufficient accuracy in order to interpret the local fossil fuel signals recorded in plants growing over a full season. By explicitly excluding these local fossil fuel influences in our simulations, we were able to isolate the effect of using different averaging kernels constructed from proxies of plant growth and from simulated crop growth. Our main conclusions are the following:

[44] 1. The influence of the day-to-day plant growth on recorded $\Delta^{14}CO_2$ signals is not negligible and should be taken into account when interpreting plant sampled $\Delta^{14}CO_2$ values.

[45] 2. In addition to a reliable crop growth model, the construction of an averaging kernel requires the local weather information for the correct growing season and in case of crops, information about the timing of particular phenology events, such as the sowing, emergence, and flowering.

[46] 3. For some plant species, in our case for maize and wheat samples at flowering, sampling after a particular phenology stage can be beneficial as it clearly defines the end of the growing period for the organs we wish to sample. The interpretation of storage organs (fruits and seeds) in cereal plants holds much higher uncertainty than of other plant parts as they are very sensitive to water limitations and grow using reallocated carbon. As growth dynamics may

differ substantially between plant species, it is important that the choice of which plant part to sample from a particular species should be made early in the planning stage of plant sampling campaigns.

[47] 4. The use of plant growth proxies that do not account for the plant development, like temperature or radiation, introduces an uncertainty that can result in a measurable (2‰) bias between predicted and observed plant $\Delta^{14}CO_2$ signature.

[48] 5. The use of an appropriate plant growth averaging kernel helps to avoid regional plant growth variations being mistakenly interpreted as local fossil fuel contribution when using integrated plant samples to learn about fossil emissions. The biases in the calculation of the fossil fuel CO_2 fraction are up to 2 ppm of fossil fuel CO_2 signal (≈10–20% of the total expected signal) when using samples from different plant parts and up to 1–1.5 ppm when not accounting for the effect of the regional weather differences on growth period and growth rate.

[49] **Acknowledgments.** This work is part of project (818.01.019), which is financed by the Netherlands Organisation for Scientific Research (NWO). Further partial support was available by NWO VIDI grant (864.08.012). We would like to further thank I. Levin and K. Schaefer for their help supplying part of the observational and modeling data used in this study.

References

Arora, V., and P. Gajri (2000), Assessment of a crop growth-water balance model for predicting maize growth and yield in a subtropical environment, *Agric. Water Manage*, *46*(2), 157–166.

Burchuladze, A., M. Chudy, I. Eristavi, S. Pagava, P. Povinec, A. Sivo, and G. Togonidze (1989), *Anthropogenic ^{14}C variations in atmospheric CO_2 and wines*, 771–776.

Ek, M., K. Mitchell, Y. Lin, E. Rogers, P. Grunmann, V. Koren, G. Gayno, and J. Tarpley (2003), Implementation of Noah land surface model advances in the National Centers for Environmental Prediction operational mesoscale Eta model, *J. Geophys. Res.*, *108*(D22), 8851, doi:10.1029/2002JD003296.

Gamnitzer, U., U. Karstens, B. Kromer, R. E. M. Neubert, H. A. J. Meijer, H. Schroeder, and I. Levin (2006), Carbon monoxide: A quantitative tracer for fossil fuel CO_2?, *J. Geophys. Res.*, *111*(D22), 302, doi:10.1029/2005JD006966.

Godwin, H. (1962), Half-life of radiocarbon, *Nature*, *195*(4845), 984.

Goudriaan, J., and H. van Laar (1994), *Modelling Potential Crop Growth Processes: Textbook With Exercises*, 238, Kluwer Academic Publishers Dordrecht, The Netherlands, monograph.

Graven, H. D., and N. Gruber (2011), Continental-scale enrichment of atmospheric $^{14}CO_2$ from the nuclear power industry: Potential impact on the estimation of fossil fuel-derived CO_2, *Atmos. Chem. Phys.*, *11*(23), 12,339–12,349, doi:10.5194/acp-11-12339-2011.

Graven, H. D., T. P. Guilderson, and R. F. Keeling (2012), Observations of radiocarbon in CO_2 at seven global sampling sites in the Scripps flask network: Analysis of spatial gradients and seasonal cycles, *J. Geophys. Res.*, *117*(D02), 303, doi:10.1029/2011JD016535.

Guérif, M., and C. Duke (1998), Calibration of the SUCROS emergence and early growth module for sugar beet using optical remote sensing data assimilation, *Eur. J. Agron.*, *9*(2-3), 127–136.

Hong, S.-Y., Y. Noh, and J. Dudhia (2006), A new vertical diffusion package with an explicit treatment of entrainment processes, *Mon Weather Rev.*, *134*(9), 2318–2341.

Hsueh, D. Y., N. Y. Krakauer, J. T. Randerson, X. Xu, S. E. Trumbore, and J. R. Southon (2007), Regional patterns of radiocarbon and fossil fuel-derived CO_2 in surface air across North America, *Geophys. Res. Lett.*, *34*(2), L02–816, doi:10.1029/2006GL027032.

Kalnay, E., et al. (1996), The NCEP/NCAR 40-year reanalysis project, *Bull. Am. Meteorol. Soc.*, *77*(3), 437–471.

Keeling, C. (1978), Atmospheric carbon-dioxide in 19th-century, *Science*, *202*(4372), 1109–1109.

Keeling, C., T. Whorf, M. Wahlen, and J. van der Plicht (1995), Interannual extremes in the rate of rise of atmospheric carbon-dioxide since 1980, *Nature*, *375*(6533), 666–670.

Kooistra, L., A. Bergsma, B. Chuma, and S. de Bruin (2009), Development of a dynamic web mapping service for vegetation productivity using Earth observation and in situ sensors in a sensor web based approach, *Sensors*, *9*, 2371–2388, doi:10.3390/s90402371.

LeQuere, C., et al. (2007), Saturation of the Southern Ocean CO_2 sink due to recent climate change, *Science*, *316*(5832), 1735–1738, doi:10.1126/science.1136188.

Levin, I., and U. Karstens (2007), Inferring high-resolution fossil fuel CO_2 records at continental sites from combined $^{14}CO_2$ and CO observations, *Tellus B*, *59*, 245–250.

Levin, I., and C. Rodenbeck (2008), Can the envisaged reductions of fossil fuel CO_2 emissions be detected by atmospheric observations? *Naturwissenschaften*, *95*(3), 203–208.

Levin, I., K. Munnich, and W. Weiss (1980), The effect of anthropogenic CO_2 and ^{14}C sources on the distribution of ^{14}C in the atmosphere, *Radiocarbon*, *22*(2), 379–391.

Levin, I., B. Kromer, M. Schmidt, and H. Sartorius (2003), A novel approach for independent budgeting of fossil fuel CO_2 over Europe by $^{14}CO_2$ observations, *Geophys. Res. Lett.*, *30*(23), 2194, doi:10.1029/2003GL018477.

Levin, I., et al. (2010), Observations and modelling of the global distribution and long-term trend of atmospheric $^{14}CO_2$, *Tellus B*, *62*(1), 26–46, doi:10.1111/j.1600-0889.2009.00446.x.

Marland, G., T. A. Boden, and R. J. Andres (2008), *Global, regional, and national fossil fuel CO_2 emissions, in trends: A compendium of data on global change*, Oak Ridge National Laboratory, U.S. Department of Energy, Oak Ridge, Tenn., U.S.A.

Meijer, H. A. J., J. van der Plicht, J. S. Gislefoss, and R. Nijdal (1995), Comparing long-term atmospheric ^{14}C and ^{3}H records near Groningen, The Netherlands with Fruholmen, Norway and Izaña, Canary Islands ^{14}C stations, *Radiocarbon*, *37*(1), 39–50.

Meijer, H. A. J., H. Smid, E. Perez, and M. G. Keizer (1996), Isotopic characterisation of anthropogenic CO_2 emissions using isotopic and radiocarbon analysis, *Phys. Chem. Earth*, *21*(5-6), 483–487.

Mook, W. G., and J. van der Plicht (1999), Reporting ^{14}C activities and concentrations, *Radiocarbon*, *41*(3), 227–239.

Olivier, J. G. J., and J. J. M. Berdowski (2001), *Global emissions sources and sinks, in Berdowski, J., Guicherit, R. and B.J. Heij, "The Climate System", pp. 33–78*, Lisse, The Netherlands.

Palstra, S. W. L., U. Karstens, H. Streurman, and H. A. J. Meijer (2008), Wine ethanol ^{14}C as a tracer for fossil fuel CO_2 emissions in Europe: Measurements and model comparison, *J. Geophys. Res.*, *113*, D21305, doi:10.1029/2008JD010282.

Peters, W., et al. (2010), Seven years of recent European net terrestrial carbon dioxide exchange constrained by atmospheric observations, *Global Change Biol.*, *16*(4), 1317–1337, doi:10.1111/j.1365-2486.2009.02078.x.

Pregger, T., Y. Scholz, and R. Friedrich (2007), *Documentation of the anthropogenic GHG emission data for Europe provided in the frame of CarboEurope GHG and CarboEurope IPFinal Report CarboEurope-IP*.

Riley, W., D. Hsueh, J. Randerson, M. L. Fischer, J. G. Hatch, D. E. Pataki, W. Wang, and M. L. Goulden (2008), Where do fossil fuel carbon dioxide emissions from California go? An analysis based on radiocarbon observations and an atmospheric transport model, *J. Geophys. Res.*, *113*, G04002, doi:10.1029/2007JG000625.

Shibata, S., E. Kawano, and T. Nakabayashi (2005), Atmospheric $^{14}CO_2$ variations in Japan during 1982–1999 based on ^{14}C measurements of rice grains, *Appl. Radiat. Isot.*, *63*(2), 285–290, doi:10.1016/j.apradiso.2005.03.011.

Singels, A., M. van den Berg, M. Smit, M. Jones, and R. van Antwerpen (2010), Modelling water uptake, growth and sucrose accumulation of sugarcane subjected to water stress, *Field Crops Res.*, *117*(1), 59–69.

Skamarock, W., J. Klemp, J. Dudhia, D. O. Gill, D. M. Barker, M. G. Duda, X.-Y. Huang, W. Wang, and J. G. Powers (2008), *A description of the Advanced Research WRF Version 3, NCAR Technical Note NCAR/TN-475+STR*.

Stephens, B. B., et al. (2007), Weak northern and strong tropical land carbon uptake from vertical profiles of atmospheric CO_2, *Science*, *316*(5832), 1732–1735, doi:10.1126/science.1137004.

Stuiver, M., and H. Polach (1977), Discussion: Reporting of ^{14}C data, *Radiocarbon*, *19*(3), 355–363.

Suess, H. (1955), Radiocarbon concentration in modern wood, *Science*, *122*, 415–417.

Tans, P. P., I. Y. Fung, and T. Takahashi (1990), Observational constraints on the global atmospheric CO_2 budget, *Science*, *247*(4949), 1431–1438.

Thoning, K., and P. Tans (1989), Atmospheric carbon dioxide at mauna loa observatory. 2. Analysis of the NOAA GMCC data 1974–1985, *J. Geophys. Res.*, *94*(D6), 8549–8565.

Tolk, L. F., W. Peters, A. G. C. A. Meesters, M. Groenendijk, A. T. Vermeulen, G. J. Steeneveld, and A. J. Dolman (2009), Modelling regional scale surface fluxes, meteorology and CO_2 mixing ratios for the Cabauw tower in the Netherlands, *Biogeosciences*, *6*(10), 2265–2280.

Turnbull, J., J. Miller, S. Lehman, and P. Tans (2006), Comparison of $^{14}CO_2$, CO, and SF_6 as tracers for recently added fossil fuel CO_2 in the atmosphere and implications for biological CO_2 exchange, *Geophys. Res. Lett.*, *33*, L01817, doi:10.1029/2005GL024213.

Turnbull, J., P. Rayner, J. Miller, T. Naegler, P. Ciais, and A. Cozic (2009), On the use of $^{14}CO_2$ as a tracer for fossil fuel CO_2: Quantifying uncertainties using an atmospheric transport model, *J. Geophys. Res.*, *114* (D22), 302, doi:10.1029/2009JD012308.

van Ittersum, M., P. Leffelaar, H. van Keulen, M. Kropff, L. Bastiaans, and J. Goudriaan (2003), On approaches and applications of the Wageningen crop models, *Eur. J. Agron.*, *18*(3-4), 201–234.

van Laar, H., J. Goudriaan, and H. V. Keulen (1997), *SUCROS97: Simulation of Crop Growth for Potential and Water-Limited Production Situations; as Applied to Spring Wheat*, 52, vol. 14, DLO Research Institute for Agrobiology and Soil Fertility and The C.T. de Wit Graduate School for Production Ecology, Wageningen, The Netherlands.

Vay, S. A., S. C. Tyler, Y. Choi, D. R. Blake, N. J. Blake, G. W. Sachse, G. S. Diskin, and H. B. Singh (2009), Sources and transport of $\Delta^{14}C$ in CO_2 within the Mexico City Basin and vicinity, *Atmos. Chem. Phys.*, *9* (14), 4973–4985.

Willmott, C. (1982), Some comments on the evaluation of model performance, *Bull. Am. Meteorol. Soc.*, *63*(11), 1309–1313.

Xevi, E., J. Gilley, and J. Feyen (1996), Comparative study of two crop yield simulation models, *Agric. Water Manage.*, *30*(2), 155–173.

Zhang, L., W. van der Werf, W. Cao, B. Li, X. Pan, and J. Spiertz (2008), Development and validation of SUCROS-cotton: A potential crop growth simulation model for cotton, *NJAS - Wageningen J. Life Sci.*, *56*, 59–83.